How good is the IMO Working List of Meteor showers? A complete analysis of the IMO Video Meteor Database

Sirko Molau, Abenstalstr. 13b, 84072 Seysdorf, Germany

Motivation

Since the start of the AKM network in 1999, which was renamed to *IMO Video Meteor Network* in 2004, plenty of single-station video data have been collected by numerous video observers. As of today, the database has grown to more than 200,000 meteor records. Until now, however, detailed analyses have only been carried out for selected meteor showers like the Perseids (Arlt, 2003) and the Taurids (Triglav-Cekada and Arlt, 2005). Most showers remained unanalysed. Short-term meteor shower outbursts were recorded, but so far they were only noticed if an observer got aware of them by chance (c.f. the October-Carmelopardalid outburst of October 5, 2005).

When the video network was established, the central aim was to cover the annual meteor shower activity within three to five years completely. This goal has been achieved at large. Since we now have the observational basis, it was time for a first complete analysis of meteor shower activity based on the video meteor database.

Theoretical background

Searching for meteor showers in a set of meteor records comes down to a pattern recognition problem. The basic formula for all *statistical* pattern recognition system is *Bayes' decision rule*:

$$R = \underset{R'}{\operatorname{argmax}}\ P(R' \mid M)$$

Bayes' rules states, that given a set of observations M (in this case: meteors), you should choose the set of classes R (in this case: radiants) such that the a-posteriori (or posterior) probability P (R | M) is maximized. Applying Bayes' rule *guarantees* minimum classification errors.

Unfortunately, the a-posteriori probability distribution P (R | M) is usually unknown and difficult to model, which is why it is often transformed according to *Bayes' Identity*:

$$P(R \mid M) = \frac{P(R) * P(M \mid R)}{P(M)}$$

Hereby, P (M | R) is the class-conditional probability distribution, and P (R) and P (M) are the a-priori (or prior) probability distributions. Hence, we can write the classification problem as:

$$R = \underset{R'}{\operatorname{argmax}}\ \frac{P(R') * P(M \mid R')}{P(M)}$$

The conditional probability distribution P (M | R), i.e. the probability that a meteor belongs to a given radiant, can be modeled easily. It is equivalent to the standard criterion for meteor shower assignment in visual observation, which is based on the radiant altitude, the distance of the meteor's backward prolongation from the radiant, the meteor velocity and the meteor length relative to the distance from the radiant (c.f. the chapter on shower association in the IMO handbook for visual observers, Rendtel et al, 1995). A closed-form analytical solution for the optimization problem is not obvious, so often iterative algorithms like *Expectation Maximization* (EM algorithm) are applied. A more simple approach is a full search over all possible radiants, selecting those, which fit to at least a pre-defined minimum number of meteors.

The a-priori probability distribution of radiants P (R) can be modeled as well. This factor captures prior knowledge about meteor showers like the fact, that radiants near the ecliptic are more probable than radiants at large ecliptical latitudes, and that meteors from radiants below the horizon of the observer are impossible. In the most simple case, P (R) is assumed to be equally distributed (i.e. all radiants have the same probability) and becomes a constant factor in the optimization problem that can be neglected.

The probability of the observation P (M) is a constant factor that can be neglected as well. Hence, detecting meteor showers comes down to finding radiants that maximize the class-conditional probability P (M | R).

A radiant is defined by a four-dimensional vector composed of the right ascension α and declination δ, the pre-atmospheric velocity v_∞ and solar longitude λ (equivalent to the time of year). During the optimization, the probabilities P (M | R) are accumulated over all meteors and all possible radiants with high resolution (i.e. small step size) in all four axes. A meteor showers radiant will manifest itself as a local probability maximum in the four dimensional space, and a meteor shower active over some period of time will cause a probability maximum which is elongated along the solar longitude axis.

Practical aspects of the implementation

Searching for elongated local maxima in a four dimensional space is not straight forward. A four-dimensional Hough transform may be applied, but the computation would be tricky and memory demanding. A possible approximation is to accumulate the probabilities P (M | R) at first for short solar longitude intervals independently, reducing the probability space to three dimensions (right ascension, declination, velocity). This part of the calculation, which is carried out by the RadFind tool, is similar to run Rainer Arlts Radiant software (Arlt, 1992) for all possible meteor shower velocities at once.

In a second step, probability maxima (radiants) are determined for each solar longitude interval. The search is straight forward, since the software simply needs to search for local peaks in the three-dimensional probability distribution.

Meteor showers are determined in a third step by looking for radiants with similar parameters (right ascension, declination, velocity) in consecutive solar longitude intervals. This search is implemented in the StrmFind tool. In addition, StrmFind tries to identify detected meteor showers using IMO‘s Working List of Meteor Showers and a set of known sporadic sources.

Detecting radiants with RadFind

The class-conditional probability distribution P (M | R) was modeled by a two-dimensional Gaussian distribution:

$$P(M \mid R) = \frac{\exp(-0.5\, D^2) * \exp(-1.5\, V^2)}{N}$$

Here, D denotes the miss distance between the backward prolongated meteor and the radiant in degree, and V the difference between the expected and the observed apparent meteor velocity in degree per second. The expected angular velocity was computed by the refined equation of Gural (1999). P (M | R) is set to zero for radiants below the horizon, or when the meteor did not fit to the radiant for other reasons (too long, moving towards the radiants). The scaling factors 0.5 and 1.5 were set empirically.

The norm factor N is necessary to make sure that each meteor contributes the same unity probability mass, which is required by probability theory. From the analysis of visual observations with the Radiant software it is known, however, that short meteors close to a radiant are strongly overweighted. Their probability mass is distributed over a few radiant bins only, whereas the probability mass of long meteors at larger radiant distances is shared by many radiant bins leaving only little probability mass for each. In fact, too slow meteors are often omitted in these analyses. For this reason, the norm factor N was neglected here, resulting in unnormalized distributions and more weight for long meteors.

Another problem arises from the imperfect meteor distribution around the radiant and the discrete sampling of radiant positions and velocities. A given meteor may cause more than one local probability maximum as depicted in Figure 1. Furthermore, strong meteor showers may mask weaker ones when their probability distributions overlap (Figure 2).

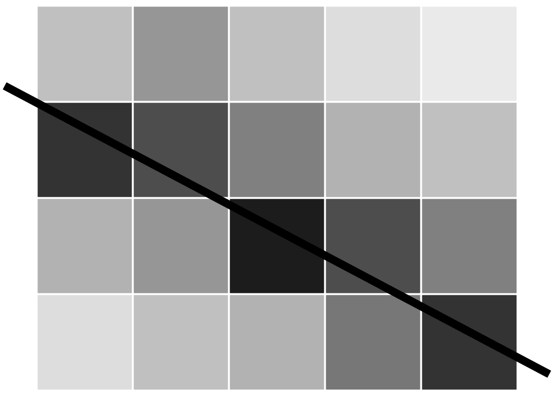

Figure 1: *The backward prolongation of one or more meteors (black line) may result in several local maxima in the discrete probability space (rectangles with different shades of grey)*

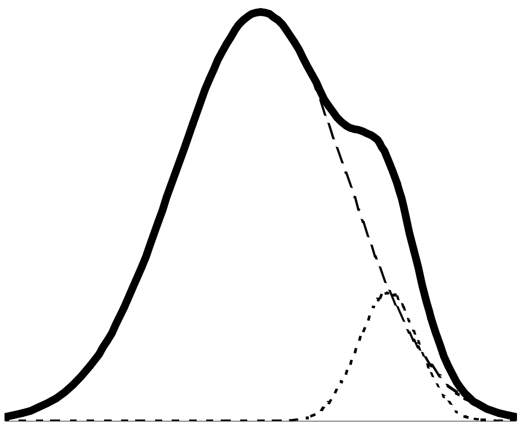

Figure 2: *Overlapping probability distributions of two showers (dotted lines) may cause that the weaker shower is masked by the stronger (thick line).*

Both problems are solved by applying an iterative algorithm. It extracts not all radiants at a time, but in each iteration only the strongest, which is subsequently removed from the data set:

- compute the global probability distribution $P(M \mid R)$ over all meteors
- loop
  - determine the strongest radiant R_G belonging to global maximum of the probability distribution
    $$R_G = \underset{R'}{\operatorname{argmax}}\ P(M \mid R')$$
  - determine the subset of meteors M_G belonging to the radiant R_G using the standard criteria for meteor shower association
  - compute the probability distribution $P_G(M_G \mid R)$ over the meteor subset
  - determine the final parameters of the strongest radiant from the meteor subset M_G
    $$R_G = \underset{R'}{\operatorname{argmax}}\ P_G(M_G \mid R')$$
  - subtract the probability distribution $P_G(M_G \mid R)$ from the overall distribution $P(M \mid R)$ and repeat the analysis for the next strongest radiant

In the example of Figure 2, the contribution of the strong radiant (large Gaussian) is removed from the overall distrubution after the first iteration, leaving only the contribution of the weak radiant (small Gaussian).

To estimate the activity of a given radiant from the available data is not straight forward. The plain number of meteor alone is a poor estimate, since the effective observing time varies significantly from one solar longitude interval to the next. The meteor number belonging to a radiant relative the overall number of meteors in this solar longitude interval is better estimate. Still it is heavily affected by other radiants. The Taurid activity profile, for example, would have a major gap during the Leonid maximum.

Therefore, the following approach was choosen: At first, all active radiants and meteors belonging to these radiants are determined. The remaining meteors are assumed to be the sporadic background, which should vary only little within a few days or weeks. The activity index of a given radiant is then defined as the ratio of the number of meteors belonging to the radiant, and the meteor number from the sporadic background. It turns out, that this measure results in accurate qualitative profiles of the meteor shower activity over time. However, it cannot be used to compare the strength of two showers, as a meteor shower that is active all night with the radiant high in the sky will have a stronger profile than a shower whose radiant rises just before dawn. To account for this effect, each meteor would need to be weighted with $\sin^{-1}$of the radiant altitude at its appearance time.

There is one case, where the activity measure in connection with the iterative radiant determination is problematic: If there are two nearby radiants with approximately the same strength like the Taurids, their activity measures with interfere: At first, the Southern Taurids show the stronger radiant. Hence, they will be extracted first from the data set, and all meteors radiating from in between the southern and northern branch will be counted as Southern Taurids. At some points, the Northern Taurids become more prominent. Now, the northern branch is extracted first and intermediate meteors are assigned to it. This explains, why between 221 and 226 degree solar longitude, the activity of these two showers seems to jump erratically.

To account for this side effect would require to repeat the meteor shower assignment for each meteor once all showers are extracted from the data set.

For the analysis presented in this paper, the following parameter setting were used:

- 360 overlapping solar longitude intervals (2° interval length, 1° shift)
- ½° step size in right ascension and declination
- 1 km/s step size in velocity

With these settings, the radiant search comes down to computing about 2 x 2 x 2.5 Million radiant probabilities for each of the almost 200,000 meteors in the database (one factor of two results from the iterative algorithm, the other from the overlapping solar longitude intervals). The calculation took about one month on two HP DL-380 Win 2003 servers with two 3 GHz dual-core CPUs each.

Detecting meteor showers with StrmFind

The output of the RadFind tool is a set of radiants for each solar longitude interval. To detect meteor showers that are active over a longer period of time, it is necessary to search subsequent solar longitude intervals for radiants with similar parameters. In this analysis, maximum deviations of 7° in the radiant position and 7 km/s in velocity were allowed for subsequent solar longitude intervals. To be reported, a meteor shower needed to be detected in at least six subsequent solar longitude intervals (all empirical values).

From the individual radiants, mean radiant position and velocity values as well as the radiant drift were determined for each shower. Then, the detected meteor showers were matched against the IMO Working List and six known sporadic sources (N/S Apex, N/S Toroidal, Helion, Anthelion). Here, at most 15° position and 15 km/s velocity deviation were accepted.
It turned out, that the number of detected meteor showers depends strongly on the parameter set. By slightly relaxing the criteria, hundreds of "meteor showers" can be „generated". To keep the list short and concentrate on the most probable showers, slighter tighter criteria than given above were applied to showers that neither belonged to the IMO Working List nor to one of the sporadic sources.

Since meteor showers have a fixed velocity, it might be useful to recompute the radiant position in the individual solar longitude intervals with the fixed mean velocity. However, this requires that the same subset of meteors is used that was assigned to the radiant before. Otherwise meteors from other showers with different velocities may strongly dilute the radiant, as they will not converge anymore at their proper radiant position.

Figures 3 and 4 show the differences in radiant position of the Perseids with and without fixed velocity. As the differences are only marginal, the position correction was not applied in the analysis presented here.

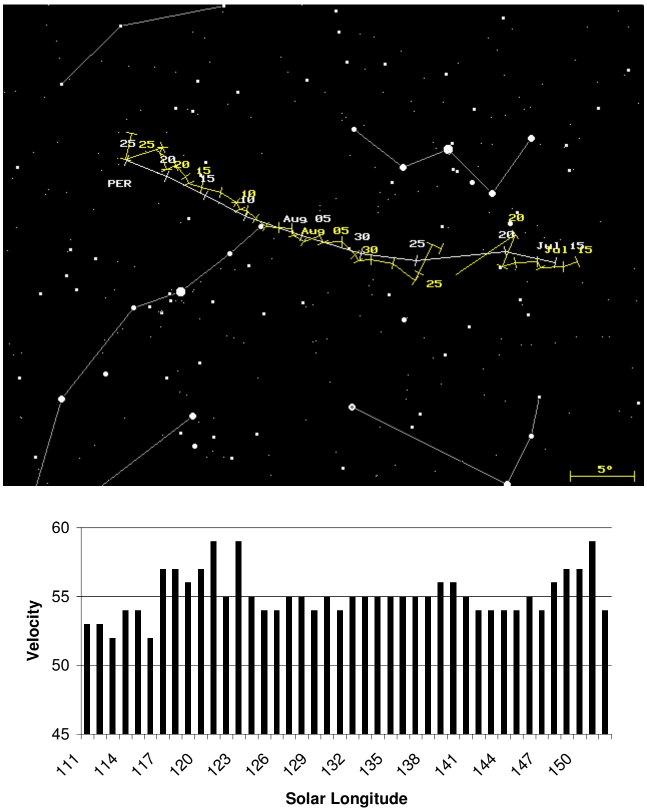

Figure 3: *Radiant position of the Perseids (upper graph) when the best velocity fit for each solar longitude interval is used (lower graph).*

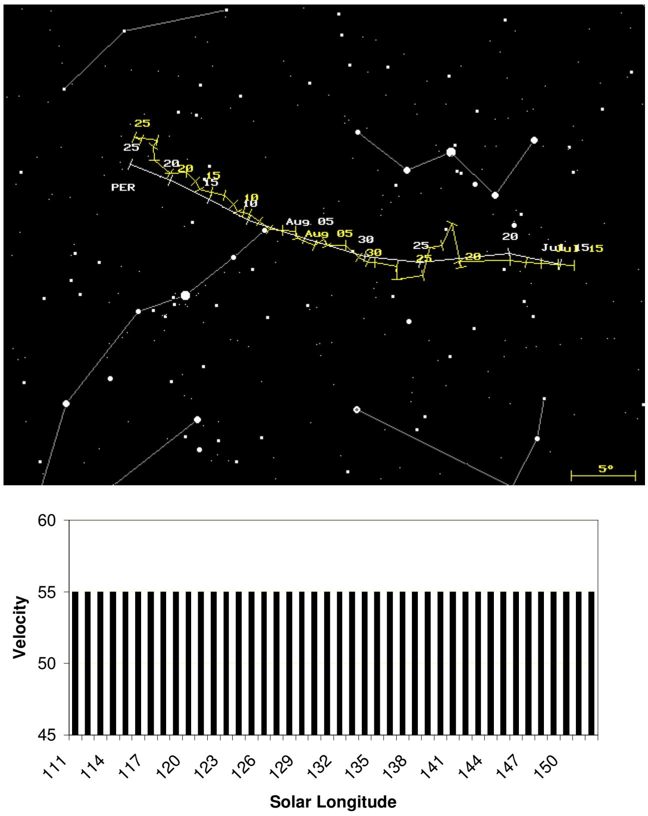

Figure 4: *Radiant position of the Perseids (upper graph) when the velocity is fixed at the average value of 55 km/s (lower graph).*

Results

The results presented in this section are based on a total of 188,068 meteors records collected in 2,146 observing nights and more than 42,500 hours effective observing time between January 1993 and February 2006. Table 1 lists all observers that contributed more than thousand video meteor records.

Table 1: *Video observers, who contributed most data to the analysis presented here.*

Observer	Country	Obs. Nights	eff. Obs. Time [h]	Meteors
Sirko Molau	Germany	1287	9354,0	64011
Jörg Strunk	Germany	921	7097,7	23213
Jürgen Rendtel	Germany	647	3823,4	17252
Ilkka Yrjölä	Finland	497	3047,5	8932
Orlando Benitez-Sanchez	Spain	488	3161,7	8464
Stane Slavec	Slovenia	418	2334,3	6383
Steve Quirk	Australia	341	3041,8	10109
Javor Kac	Slovenia	328	2305,5	3735
Detlef Koschny	Netherlands	312	1947,8	8395
Stephen Evans	UK	254	1508,6	6366
Mirko Nitschke	Germany	213	942,5	5430
Stefan Ueberschaer	Germany	173	882,3	1684
Ulrich Sperberg	Germany	133	887,3	4005
Rosta Stork	Czech Rep.	52	701,6	5621
Rob McNaught	Australia	50	395,5	5102
Enrico Stomeo	Italy	30	154,0	1047

Figure 5 shows the distribution of meteors over solar longitude. As expected, most meteor records come from the second half of the year. In addition, there are strong peaks caused by the Perseids, Leonids, and Geminids. The number of meteors varies between 200 (March 7 / solar longitude 348°) and 13,021 meteors (November 19 / solar longitude 236°) per interval.

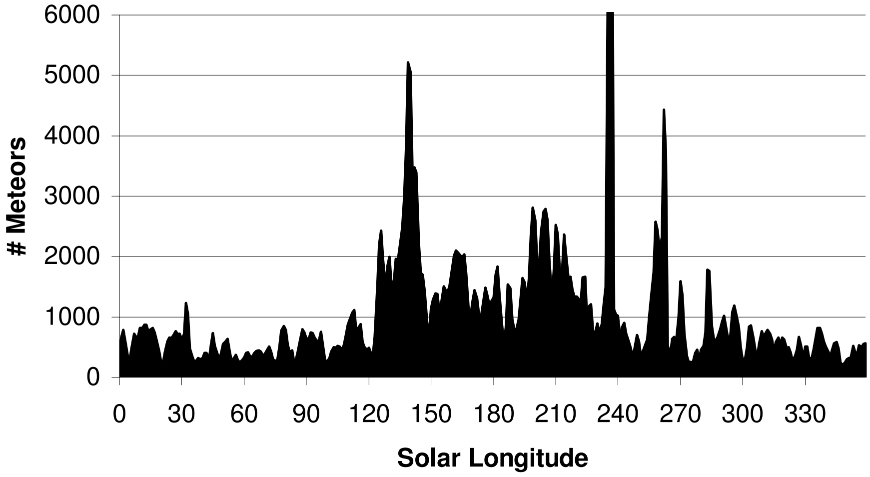

Figure 5: *Distribution of meteors over solar longitude.*

With the settings described above, 54 meteor shower were found. 24 of these were known showers from the recently updated IMO Working List (Arlt and Rendtel, 2006), among them the Antihelion source, which can be detected numerous times in the course of the year. Four sporadic sources could be identified, and the remaining 26 showers did neither fit to the IMO Working List nor to any sporadic source.

Table 2 gives the details of the detected meteor showers, ordered by their appearance date. The columns are as follows:

- ID – arbitrary identifier from the detection algorithm
- Period of Activity – solar longitude interval in which a radiant was detected, the corresponding dates, and the overall number of meteors belonging to the shower (in parenthesis are the reference values from the IMO Working List, if available).
  Beware that the given meteor number is about two times the real number of meteors, since due to the overlapping solar longitude intervals most meteors were counted twice.
- Maximum Activity - solar longitude and date of maximum activity, maximum activity index (in parenthesis are the reference values from the IMO Working List, if available).
- Properties – right ascension, declination, and velocity of the meteor showers at the time of maximum activity (in parenthesis are the reference values from the IMO Working List and for the sporadic source at the *observed* time of maximum activity, if available)
- Drift – average drift in right ascension and declination per day (in parenthesis are the reference values from the IMO Working List or for the sporadic source, if available). Beware that the radiant position in solar longitude intervals with low activity is difficult to determine, which is why the drift values may contain large errors.
- Remarks - name of the shower or sporadic source, if known, and further comments

Figure 6 contains activity graphs for all showers from the IMO working list, and a number of other interesting showers. Please note, that the scale of the y-axis varies for strong showers.

Table 2: *List of detected meteor showers.*

ID	Period of Activity			Maximum Activity		Properties				Drift		Remark	
	λ [°]	Date	# Met.	λ [°]	Date	α [°]	δ [°]	Vel. [km/s]	Act. %	α °/day	δ °/day	Name	#
83	276-292 (280-284)	Dec 28-Jan 12 (Jan 01-Jan 05)	2177	283 (282)	Jan 04 (Jan 03)	230.2 (230.8)	49.5 (48.8)	41 (41)	96.4	1.0 (0.8)	-0.1 (-0.2)	QUA	1
84	278-286 (260-303)	Dec 30-Jan 07 (Dec 12-Jan 23)	356	280 (267)	Jan 01 (Dec 19)	172.1 (186.4)	25.0 (20.1)	58 (65)	10.3	0.6 (0.8)	0.0 (-0.3)	(COM)	2
85	279-287	Dec 31-Jan 07	292	285	Jan 06	117.6 (117.0)	18.5 (19.0)	28 (30)	8.2	2.1 (1.0)	0.3 (-0.2)	ANT	-
86	280-285	Jan 01-Jan 06	118	282	Jan 03	146.2	24.5	55	4.7	1.2	-0.5	-	3
87	280-285	Jan 01-Jan 06	56	282	Jan 03	176.0 (182.7)	-23.0 (-23.0)	62 (60)	3.2	-1.4 (0.9)	-1.5 (-0.4)	S Apex	-
88	281-286	Jan 02-Jan 07	90	283	Jan 04	130.8 (120.1)	27.5 (20.6)	39 (30)	4.2	0.0 (1.0)	-1.6 (-0.2)	Anthel.	-
89	282-289	Jan 03-Jan 09	128	283	Jan 04	128.0	-12.5	39	3.7	0.4	-0.1	-	4
90	288-294	Jan 08-Jan 14	127	294	Jan 14	127.9 (126.0)	10.0 (17.2)	28 (30)	3.8	-1.4 (1.0)	-2.3 (-0.2)	ANT	-
91	293-299 (260-303)	Jan 13-Jan 19 (Dec 12-Jan 23)	373	296 (267)	Jan 16 (Dec 19)	186.1 (199.2)	18.5 (15.3)	60 (65)	7.7	-1.1 (0.8)	-0.2 (-0.3)	(COM)	2
92	307-316	Jan 27-Feb 05	213	316	Feb 05	156.9 (149.0)	9.0 (11.0)	36 (30)	5.9	0.3 (1.0)	-0.8 (-0.4)	ANT	-
93	311-316	Jan 31-Feb 05	89	313	Feb 02	158.4	-11.0	42	3.7	0.0	-0.4	-	-
94	316-323	Feb 05-Feb 12	204	323	Feb 12	151.8 (156.0)	12.0 (8.2)	30 (30)	8.1	0.6 (1.0)	0.6 (-0.4)	ANT	-
95	328-337	Feb 17-Feb 26	282	336	Feb 25	162.2 (169.0)	2.5 (3.0)	27 (30)	7.8	-1.1 (1.0)	-0.7 (-0.4)	ANT	-
1	357-2	Mar 18-Mar 23	197	1	Mar 22	185.6 (194.0)	1.5 (-6.8)	30 (30)	8.2	-0.6 (1.0)	1.4 (-0.4)	ANT	-
2	9-17	Mar 30-Apr 07	190	10	Mar 31	276.2 (277.2)	40.5 (26.8)	41 (35)	4.7	0.1 (0.7)	-0.5 (0.1)	N Toroidal	5
3	10-16	Mar 31-Apr 06	163	16	Apr 06	201.9	64.0	18	5.2	-1.8	0.3	-	6
4	14-19	Apr 04-Apr 09	118	18	Apr 08	220.1 (211.0)	-8.0 (-12.9)	37 (30)	3.4	2.3 (1.0)	-0.4 (-0.3)	ANT	-
5	26-33	Apr 16-Apr 23	241	33	Apr 23	223.3	-24.0	29	8.2	0.0	-0.7	ANT	-

						(226.0)	(-17.4)	(30)		(1.0)	(-0.3)		
6	27-33	Apr 17-Apr 23	406	29	Apr 19	217.6 (222.0)	-17.5 (-16.2)	29 (30)	16.8	-1.1 (1.0)	-0.2 (-0.3)	ANT	7
7	27-35 (26-35)	Apr 17-Apr 25 (Apr 16-Apr 25)	1216	33 (32)	Apr 23 (Apr 22)	273.1 (272.1)	33.0 (34.0)	45 (49)	73.5	0.3 (1.1)	-0.2 (0.0)	LYR	-
8	37-45	Apr 27-May 06	246	44	May 05	241.4 (237.0)	-16.0 (-20.7)	30 (30)	10.3	1.1 (1.0)	0.4 (-0.3)	ANT	-
9	37-58 (29-67)	Apr 27-May 19 (Apr 19-May 29)	959	45 (44)	May 06 (May 05)	337.5 (338.9)	-1.0 (-0.6)	59 (66)	35.9	0.6 (0.9)	0.4 (0.4)	ETA	8
10	49-56 (42-51)	May 10-May 17 (May 03-May 12)	203	50 (48)	May 11 (May 09)	291.2 (289.0)	43.0 (44.0)	43 (44)	10.0	0.7 (1.0)	0.2 (0.0)	ELY	-
11	61-68	May 22-May 30	192	67	May 29	254.2 (260.0)	-15.5 (-23.3)	30 (30)	8.3	-0.2 (1.0)	0.3 (-0.1)	ANT	-
12	74-83	Jun 05-Jun 14	566	75	Jun 06	260.2 (267.0)	-23.0 (-23.9)	27 (30)	16.4	0.7 (1.0)	-1.0 (0.1)	ANT	9
13	85-108	Jun 16-Jul 10	683	92	Jun 24	9.1 (353.6)	21.0 (19.1)	61 (60)	9.8	0.6 (0.9)	0.5 (0.4)	N Apex	-
14	86-94	Jun 17-Jun 26	317	87	Jun 18	274.0 (279.0)	-29.5 (-22.7)	26 (30)	9.8	1.2 (1.0)	2.0 (0.1)	ANT	-
14a	89-93	Jun 20-Jun 25	58	92 (95)	Jun 24 (Jun 27)	215.9 (222.5)	38.5 (48.2)	15 (18)	5.4	0.0 (0.4)	1.5 (-0.2)	JBO	10
15	91-99	Jun 23-Jul 01	189	99	Jul 01	282.7 (291.0)	-26.5 (-21.5)	24 (30)	5.5	0.5 (1.0)	0.6 (0.1)	ANT	-
16	91-98	Jun 23-Jun 30	288	93	Jun 25	304.0	-6.5	40	8.7	0.9	0.3	-	11
17	92-98	Jun 24-Jun 30	97	97	Jun 29	290.4 (289.0)	-20.5 (-21.7)	32 (30)	4.0	-1.2 (1.0)	1.7 (0.1)	ANT	-
18	100-105	Jul 02-Jul 07	123	105	Jul 07	25.4	46.5	56	6.9	-0.3	0.5	-	-
19	106-112	Jul 08-Jul 15	251	108	Jul 10	315.3	-4.0	40	8.7	0.6	0.6	-	12
20	108-139 (101-142)	Jul 10-Aug 12 (Jul 03-Aug 15)	2440	128 (127)	Jul 31 (Jul 30)	306.7 (309.0)	-9.5 (-9.7)	24 (23)	16.4	0.6 (1.0)	0.2 (0.3)	CAP	13
21	110-118	Jul 13-Jul 21	498	117	Jul 20	21.0 (17.0)	36.0 (28.9)	62 (60)	10.9	0.6 (1.0)	0.4 (0.4)	N Apex	-
22	111-118 (114-151)	Jul 14-Jul 21 (Jul 17-Aug 24)	523	117 (139)	Jul 20 (Aug 12)	9.1 (17.4)	53.0 (53.6)	57 (59)	13.4	1.5 (1.3)	0.4 (0.2)	PER	14
23	113-119	Jul 16-Jul 22	88	118	Jul 21	314.6	-17.5	31	5.6	1.0	-1.0	ANT	-

						(310.4)	(-16.8)	(30)		(0.9)	(0.2)		
24	114-119	Jul 17-Jul 22	159	116	Jul 19	322.7	-2.0	39	7.2	0.1	0.4	-	15
25	117-158 (110-146)	Jul 20-Sep 01 (Jul 13-Aug 19)	4577	128 (125)	Jul 31 (Jul 28)	341.6 (342.0)	-16.5 (-15.1)	41 (41)	45.0	0.8 (1.0)	0.3 (0.3)	SDA	16
26	119-153 (114-151)	Jul 22-Aug 26 (Jul 17-Aug 24)	21157	140 (139)	Aug 13 (Aug 12)	46.5 (47.3)	57.5 (58.2)	56 (59)	355.6	1.3 (1.3)	0.3 (0.2)	PER	17
27	122-135	Jul 25-Aug 08	853	133	Aug 06	43.4 (33.3)	39.5 (34.7)	60 (60)	10.0	0.8 (1.1)	-0.3 (0.3)	N Apex	-
28	122-128	Jul 25-Jul 31	155	122	Jul 25	325.8 (314.0)	-22.5 (-16.0)	28 (30)	7.2	-1.7 (0.9)	1.5 (0.2)	ANT	-
29	126-131 (101-142)	Jul 29-Aug 04 (Jul 03-Aug 15)	133	128 (127)	Jul 31 (Jul 30)	298.1 (309.0)	-3.5 (-9.7)	22 (23)	3.6	0.6 (1.0)	0.6 (0.3)	(CAP)	18
30	127-133	Jul 30-Aug 06	185	130	Aug 02	334.7 (323.0)	-15.5 (-12.8)	28 (30)	4.3	1.3 (1.0)	0.6 (0.4)	ANT	-
31	133-139 (114-151)	Aug 06-Aug 12 (Jul 17-Aug 24)	164	139 (139)	Aug 12 (Aug 12)	47.9 (46.0)	64.0 (58.0)	50 (59)	3.4	3.9 (1.3)	0.5 (0.2)	(PER)	19
32	133-145 (131-152)	Aug 06-Aug 18 (Aug 04-Aug 25)	802	144 (144)	Aug 17 (Aug 17)	274.6 (286.0)	58.0 (59.0)	24 (25)	5.8	-0.5 (0.0)	0.9 (0.0)	KCG	20
33	135-153	Aug 08-Aug 26	1403	148	Aug 21	350.2 (344.3)	3.5 (-6.7)	37 (30)	10.5	0.7 (0.9)	0.3 (0.4)	Anthel.	-
34	137-143	Aug 10-Aug 16	387	143	Aug 16	336.3 (336.0)	-4.0 (-7.6)	35 (30)	4.8	1.5 (1.0)	0.3 (0.4)	ANT	-
35	139-144	Aug 12-Aug 17	254	142	Aug 15	40.2 (43.2)	36.0 (37.5)	54 (60)	5.7	1.4 (1.1)	1.5 (0.3)	N Apex	-
36	140-151	Aug 13-Aug 24	376	149	Aug 22	306.1	-10.5	19	3.5	-1.0	-0.8	-	21
37	146-153 (131-152)	Aug 19-Aug 26 (Aug 04-Aug 25)	405	151 (144)	Aug 24 (Aug 17)	277.2 (286.0)	60.5 (59.0)	26 (25)	7.3	-1.7 (0.0)	0.2 (0.0)	KCG	20
38	146-156	Aug 19-Aug 30	529	151	Aug 24	58.3 (53.6)	41.0 (39.8)	57 (60)	8.9	0.1 (1.2)	-2.2 (0.2)	N Apex	-
39	147-153 (114-151)	Aug 20-Aug 26 (Jul 17-Aug 24)	196	153 (139)	Aug 26 (Aug 12)	35.1 (64.2)	62.0 (60.8)	50 (59)	7.3	-1.1 (1.3)	-1.2 (0.2)	(PER)	19
40	151-156	Aug 24-Aug 30	88	156	Aug 30	74.4 (67.5)	14.5 (1.6)	65 (60)	2.4	1.1 (0.9)	1.7 (0.1)	S Apex	-
41	153-158	Aug 26-Sep 01	172	154	Aug 27	291.5	64.5	30	4.7	-1.8	-1.2	-	22
41a	156-160	Aug 30-Sep 03	323	158	Sep 01	68.1	47.5	69	6.9	-0.1	0.2	AUR	23

	(152-165)	(Aug 25-Sep 8)		(158)	(Sep 01)	(84.0)	(42.0)	(66)		(1.0)	(0.4)		
42	153-165	Aug 26-Sep 08	1015	162	Sep 05	357.9 (-5.0)	4.0 (-1.0)	31 (30)	8.0	0.8 (1.0)	0.6 (0.4)	ANT	-
43	155-165	Aug 28-Sep 08	680	163	Sep 06	66.1 (74.0)	-3.0 (2.5)	58 (60)	6.4	0.0 (0.9)	-0.1 (0.1)	S Apex	-
44	155-160	Aug 28-Sep 03	80	158	Sep 01	260.5	82.5	38	2.3	-0.7	1.4	-	24
45	155-162	Aug 28-Sep 05	113	158	Sep 01	110.5	38.5	52	1.6	1.4	-1.5	-	-
46	158-163	Sep 01-Sep 06	227	162	Sep 05	10.5 (357.2)	-3.5 (-1.2)	39 (30)	3.5	-0.2 (0.9)	-1.1 (0.4)	Anthel.	-
47	162-170 (162-174)	Sep 05-Sep 13 (Sep 05-Sep 17)	1067	167 (166)	Sep 10 (Sep 09)	47.6 (60.1)	39.0 (47.1)	61 (64)	10.7	1.7 (1.1)	0.3 (0.1)	SPE	25
48	164-169	Sep 07-Sep 12	272	165	Sep 08	9.5 (-2.0)	1.0 (0.2)	35 (30)	5.6	0.8 (1.0)	-0.3 (0.4)	ANT	-
49	166-173	Sep 09-Sep 16	220	170	Sep 13	113.6	56.0	53	4.5	2.6	-0.1	-	-
50	167-175	Sep 10-Sep 18	337	171	Sep 14	356.7 (4.0)	-3.5 (2.6)	25 (30)	7.0	0.6 (1.0)	0.0 (0.4)	ANT	-
51	170-180	Sep 13-Sep 23	865	178	Sep 21	14.1 (11.0)	6.5 (5.4)	32 (30)	10.3	1.0 (1.0)	0.5 (0.4)	ANT	-
52	173-180	Sep 16-Sep 23	465	178	Sep 21	73.7 (88.1)	8.0 (3.4)	60 (60)	7.1	0.4 (0.9)	0.5 (0.0)	S Apex	-
53	180-244 (182-243)	Sep 23-Nov 26 (Sep 25-Nov 25)	10050	226	Nov 09	55.9 (55.1)	15.0 (14.9)	30 (27)	31.4	0.7 (0.9)	0.2 (0.1)	STA	26
54	181-187	Sep 24-Sep 30	432	184	Sep 27	81.1	7.0	59	6.6	1.4	-0.1	-	-
55	186-192	Sep 29-Oct 05	156	191	Oct 04	80.4 (114.1)	82.5 (72.5)	44 (35)	3.4	-13.8 (2.1)	-0.1 (-0.2)	N Toroidal	-
56	187-192 (182-210)	Sep 30-Oct 05 (Sep 25-Oct 24)	179	190 (197)	Oct 03 (Oct 10)	18.8 (24.4)	16.5 (12.9)	32 (29)	6.0	-0.3 (0.8)	-1.7 (0.3)	NTA	27
57	190-228 (189-224)	Oct 03-Nov 11 (Oct 02-Nov 07)	11804	209 (207)	Oct 23 (Oct 21)	96.0 (96.4)	15.5 (16.2)	61 (66)	93.6	0.8 (0.7)	0.1 (0.1)	ORI	28
58	192-208 (200-213)	Oct 05-Oct 22 (Oct 14-Oct 27)	1550	200 (204)	Oct 14 (Oct 18)	96.4 (98.0)	27.5 (27.0)	64 (70)	10.6	0.7 (1.0)	-0.5 (0.0)	EGE	29
59	193-198	Oct 06-Oct 11	200	194	Oct 07	79.0 (120.2)	82.0 (72.0	42 (35	4.3	1.7 (2.0)	0.0 (0.2)	N Toroidal	30
60	193-199 (175-197)	Oct 06-Oct 12 (Sep 18-Oct 10)	374	196 (191)	Oct 09 (Oct 04)	105.8 (93.0)	46.0 (49.0)	64 (64)	7.9	2.4 (1.0)	0.8 (0.0)	DAU	31

61	197-202	Oct 10-Oct 16	141	199	Oct 12	247.9	82.0	35	2.1	-3.6	0.9	-	24
62	202-250 (211-243)	Oct 16-Dec 02 (Oct 25-Nov 25)	4532	227 (227)	Nov 10 (Nov 10)	56.6 (56.0)	22.0 (22.0)	31 (29)	31.2	0.7 (0.9)	0.1 (0.2)	NTA	32
63	203-213 (205-213)	Oct 17-Oct 27 (Oct 19-Oct 27)	469	210 (210)	Oct 24 (Oct 24)	161.3 (162.0)	36.0 (37.0)	56 (62)	6.8	1.1 (1.0)	-0.3 (-0.4)	LMI	-
64	203-212 (189-224)	Oct 17-Oct 26 (Oct 02-Nov 07)	309	210 (207)	Oct 24 (Oct 21)	104.4 (97.1)	11.0 (16.3)	59 (66)	4.7	-0.8 (0.7)	-0.1 (0.1)	(ORI)	33
65	210-221	Oct 24-Nov 04	569	220	Nov 03	148.9 (139.0)	28.0 (36.9)	63 (60)	6.9	0.8 (1.1)	-0.2 (-0.3)	N Apex	-
66	212-218 (211-243)	Oct 26-Nov 01 (Oct 25-Nov 25)	115	218 (227)	Nov 01 (Nov 10)	33.6 (47.9)	18.0 (14.1)	26 (27)	2.7	-0.4 (0.9)	-0.6 (0.1)	STA	34
67	213-221	Oct 27-Nov 04	324	217	Oct 31	120.7	16.0	60	6.0	-0.7	0.3	-	-
68	223-228	Nov 06-Nov 11	343	225	Nov 08	145.8 (144.5)	44.5 (35.3)	58 (60)	10.3	2.9 (1.1)	-0.9 (-0.3)	N Apex	-
69	225-232	Nov 08-Nov 15	204	226	Nov 09	24.6	26.5	20	5.9	0.2	1.0	-	35
70	225-246 (227-241)	Nov 08-Nov 28 (Nov 10-Nov 23)	18872	236 (234)	Nov 19 (Nov 17)	154.2 (152.4)	21.5 (21.2)	64 (71)	226.3	0.6 (0.7)	-0.4 (-0.4)	LEO	36
71	232-237 (211-243)	Nov 15-Nov 20 (Oct 25-Nov 25)	184	234 (227)	Nov 17 (Nov 10)	74.5 (62.3)	30.0 (23.4)	35 (29)	5.2	2.6 (0.9)	-0.7 (0.2)	NTA	37
72	234-253 (245-265)	Nov 17-Dec 05 (Nov 27-Dec 17)	915	246 (257)	Nov 28 (Dec 09)	90.8 (93.1)	15.5 (8.0)	44 (42)	11.8	0.8 (0.9)	0.1 (0.0)	MON	38
73	241-247	Nov 23-Nov 29	167	247	Nov 29	198.6 (187.2)	64.5 (53.4)	43 (35)	7.4	-2.3 (0.8)	-0.7 (-0.4)	N Toroidal	-
74	248-272 (251-263)	Nov 30-Dec 24 (Dec 03-Dec 15)	1216	257 (260)	Dec 09 (Dec 12)	126.6 (125.6)	2.5 (2.6)	56 (58)	13.6	0.9 (0.8)	-0.2 (-0.2)	HYD	39
75	248-266 (255-265)	Nov 30-Dec 18 (Dec 07-Dec 17)	10560	262 (262)	Dec 14 (Dec 14)	113.8 (112.0)	32.0 (33.0)	36 (35)	296.8	1.1 (1.0)	-0.1 (-0.1)	GEM	40
76	252-277 (260-303)	Dec 04-Dec 29 (Dec 12-Jan 23)	1658	268 (267)	Dec 20 (Dec 19)	161.3 (176.8)	30.5 (23.7)	59 (65)	16.5	0.8 (0.8)	-0.3 (-0.3)	COM	41
77	254-267 (245-265)	Dec 06-Dec 19 (Nov 27-Dec 17)	692	254 (257)	Dec 06 (Dec 09)	98.6 (100.3)	8.5 (8.0)	41 (42)	9.8	0.8 (0.9)	-0.4 (0.0)	MON	42
78	254-271	Dec 06-Dec 23	656	268	Dec 20	209.2 (203.9)	55.5 (45.4)	44 (35)	4.3	-1.3 (0.8)	-0.1 (-0.4)	N Toroidal	-
79	255-260	Dec 07-Dec 12	304	260	Dec 12	83.0 (93.0)	19.0 (23.0)	26 (30)	9.0	-2.4 (1.0)	2.2 (0.0)	ANT	-

80	257-262	Dec 09-Dec 14	220	257	Dec 09	178.8 (176.4)	35.0 (23.4)	53 (60)	6.5	0.0 (0.9)	0.7 (-0.4)	N Apex	-
81	257-264 (260-303)	Dec 09-Dec 16 (Dec 12-Jan 23)	201	264 (267)	Dec 16 (Dec 19)	173.9 (173.6)	25.5 (24.9)	64 (65)	7.1	3.2 (0.8)	0.4 (-0.3)	(COM)	2
82	267-272	Dec 19-Dec 24	131	268	Dec 20	202.2	8.5	62	3.4	1.3	0.0	-	-
82a	268-272 (265-274)	Dec 20-Dec 24 (Dec 17-Dec 26)	695	271 (270)	Dec 23 (Dec 22)	220.2 (217)	75.0 (74.8)	32 (33)	36.1	5.1 (0.0)	0.1 (0.4)	URS	-

Remarks:

[1] much longer activity interval than in the IMO Working List
[2] similar to the radiant of COM
[3] narrow radiant, well-shaped activity profile
[4] no clear activity profile, almost constant activity
[5] no clear activity profile
[6] relative compact radiant at high declination, conspiciously slow, no clear activity profile
[7] remarkably strong activity with a clear peak
[8] asymmetric profile: steep ascending, shallow descending branch; significantly shorter activity interval than in the IMO Working List
[9] remarkably strong activity with a clear peak
[10] noticable activity only at 92° solar longitude, radiant more than 10° north of the expected position
[11] almost constant, relatively strong activity
[12] probably the ascending branch of shower 24
[13] almost no ascending, but slow descending branch
[14] early part of the Perseids
[15] probably the descending branch of shower 19
[16] the only clear shower from the Aquarid complex, activity possibly ends at 145° solar longitude
[17] well-known extremely long ascending branch with activity plateau at 134-137° solar longitude
[18] similar to the radiant of CAP
[19] similar to the radiant of PER
[20] much larger radiant drift than in the IMO Working List
[21] conspiciously slow, no clear activity profile
[22] no clear activity profile
[23] very short activity interval, radiant far from the expected position
[24] weak radiant close to the north equatorial pole
[25] strong radiant more than 10° south-west of the expected position
[26] until 220-225° solar longitude stronger than NTA
[27] early branch of NTA
[28] almost perfect Gaussian activity profile
[29] significantly earlier active than in the IMO Working List
[30] related to October-Camelopardalids?
[31] no clear activity profile, radiant far east from the expected position
[32] starting from 220-225° solar longitude stronger than STA
[33] similar to the radiant of ORI
[34] similar to the radiant of STA
[35] conspiciously slow, almost constant activity
[36] strong peak and weak background component
[37] similar to the radiant of NTA
[38] well-defined radiant motion just as expected, but 10° north-west of the expected position
[39] activity possibly ends at 266° solar longitude
[40] activity interval much longer than in the IMO Workling List, asymmetric profile with shallow ascending and step descending branch
[41] well-defined radiant at the expected position, but more than one month behind in time
[42] ascending branch missing
[43] similar to the radiant of COM

Shower 83 (QUA)

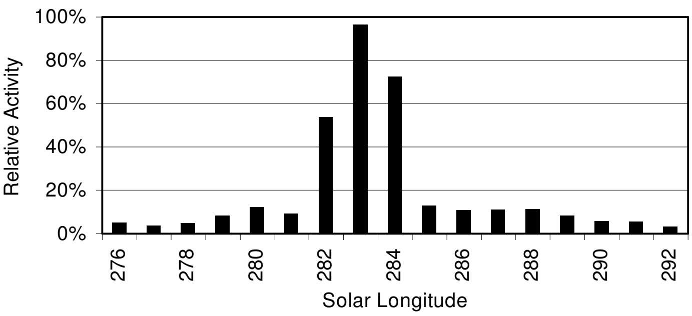

Shower 86

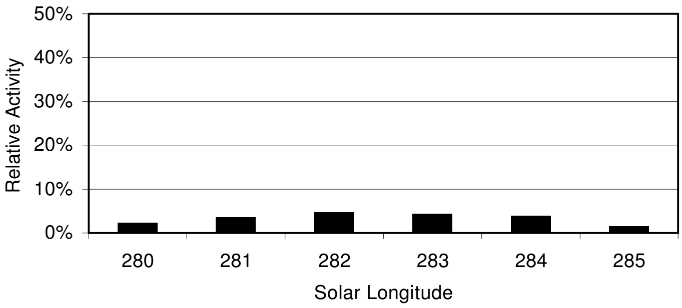

Shower 6 (ANT)

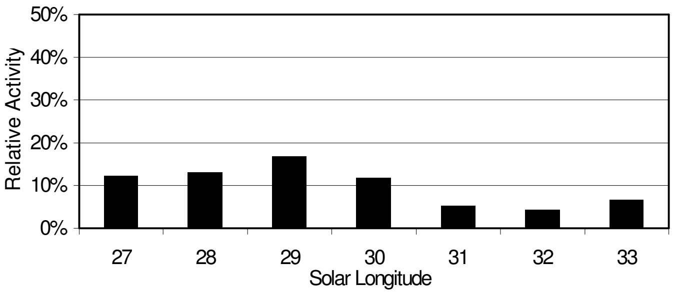

Shower 7 (LYR)

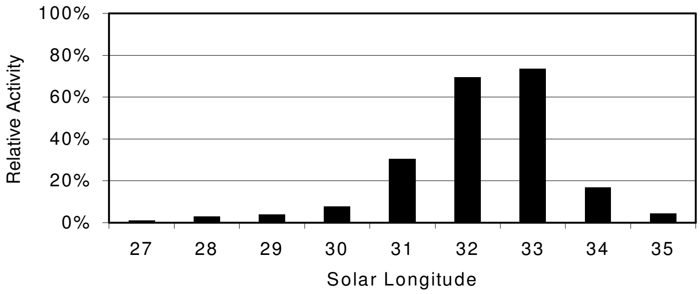

Shower 9 (ETA)

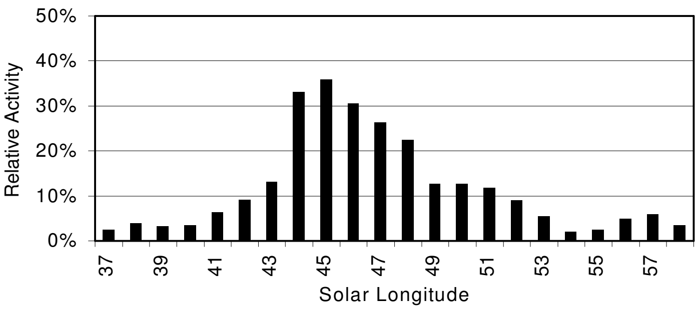

Shower 10 (ELY)

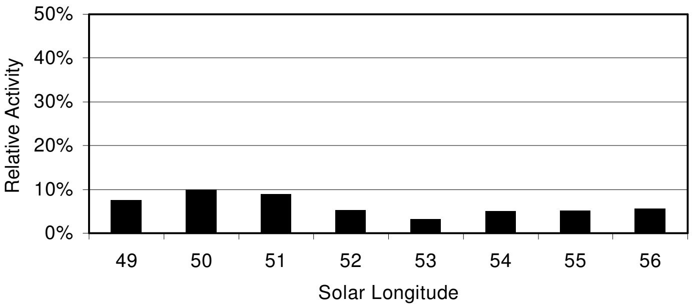

Shower 14a (JBO)

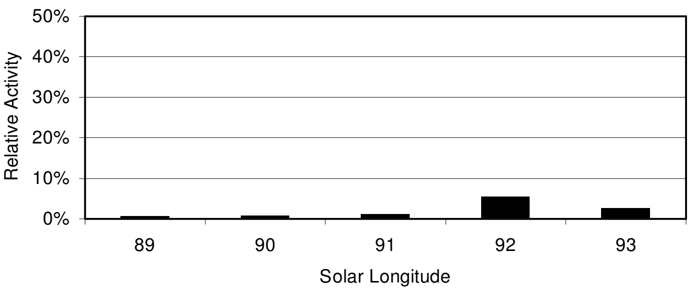

Shower 16

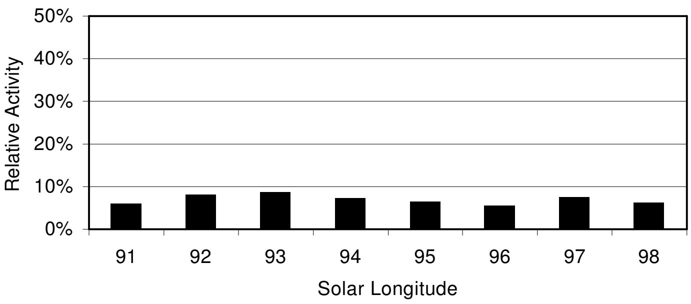

Shower 19

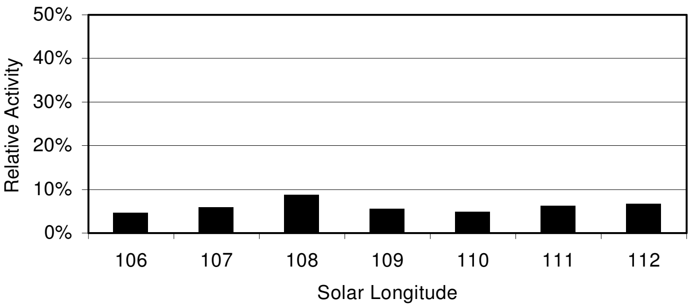

Shower 20 (CAP)

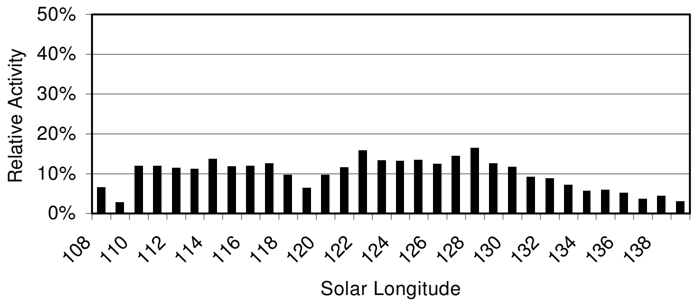

Shower 22/26 (Per)

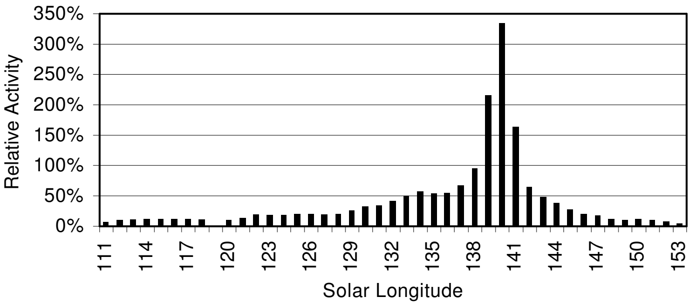

Shower 24

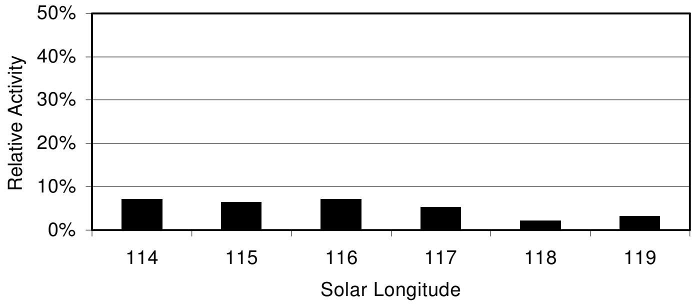

Shower 25 (SDA)

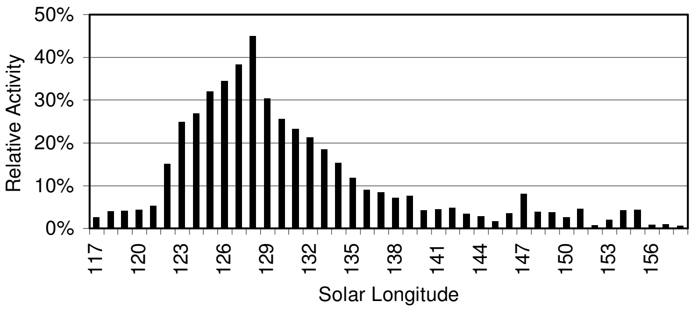

Shower 32/37 (KCG)

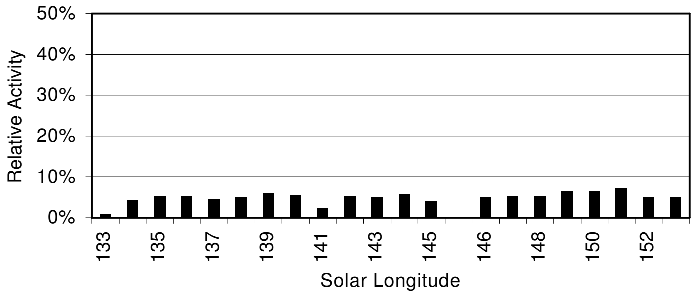

Shower 41a (AUR)

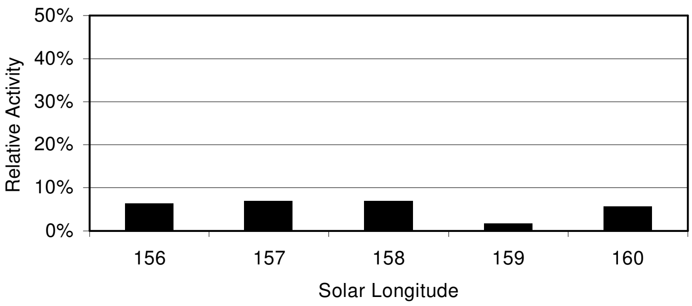

Shower 47 (SPE)

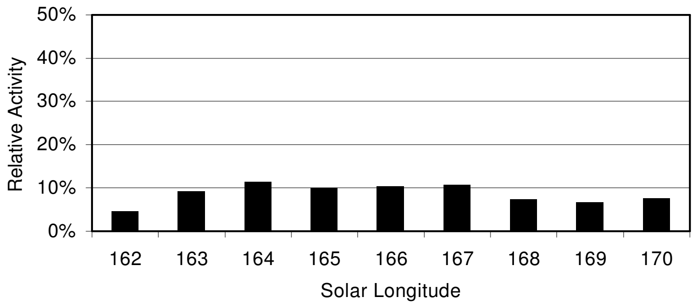

Shower 53 (STA)

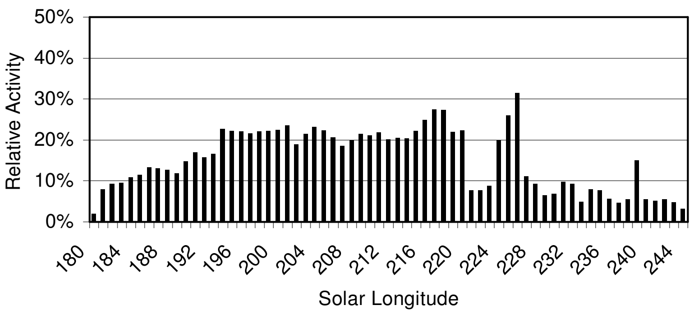

Shower 56/62 (NTA)

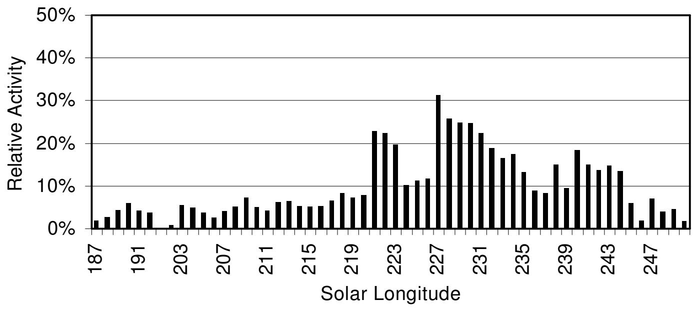

Shower 53/56/62 (NTA+STA)

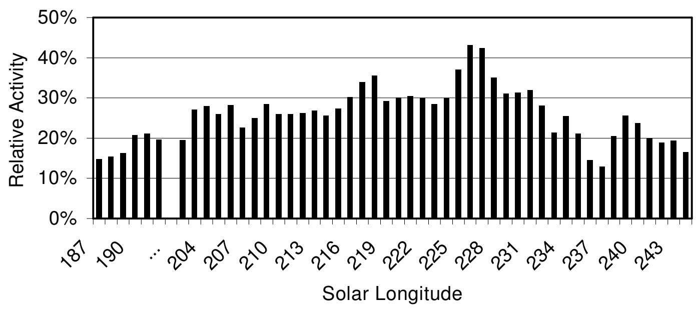

Shower 57 (ORI)

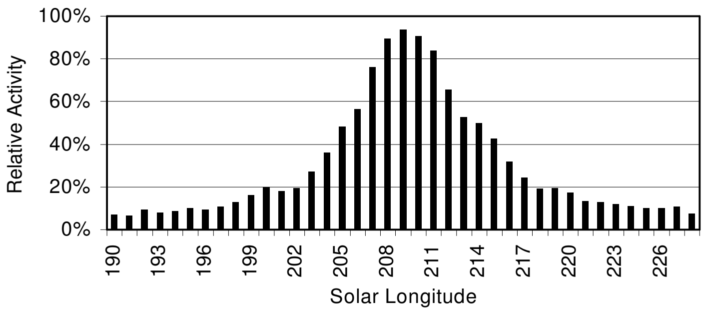

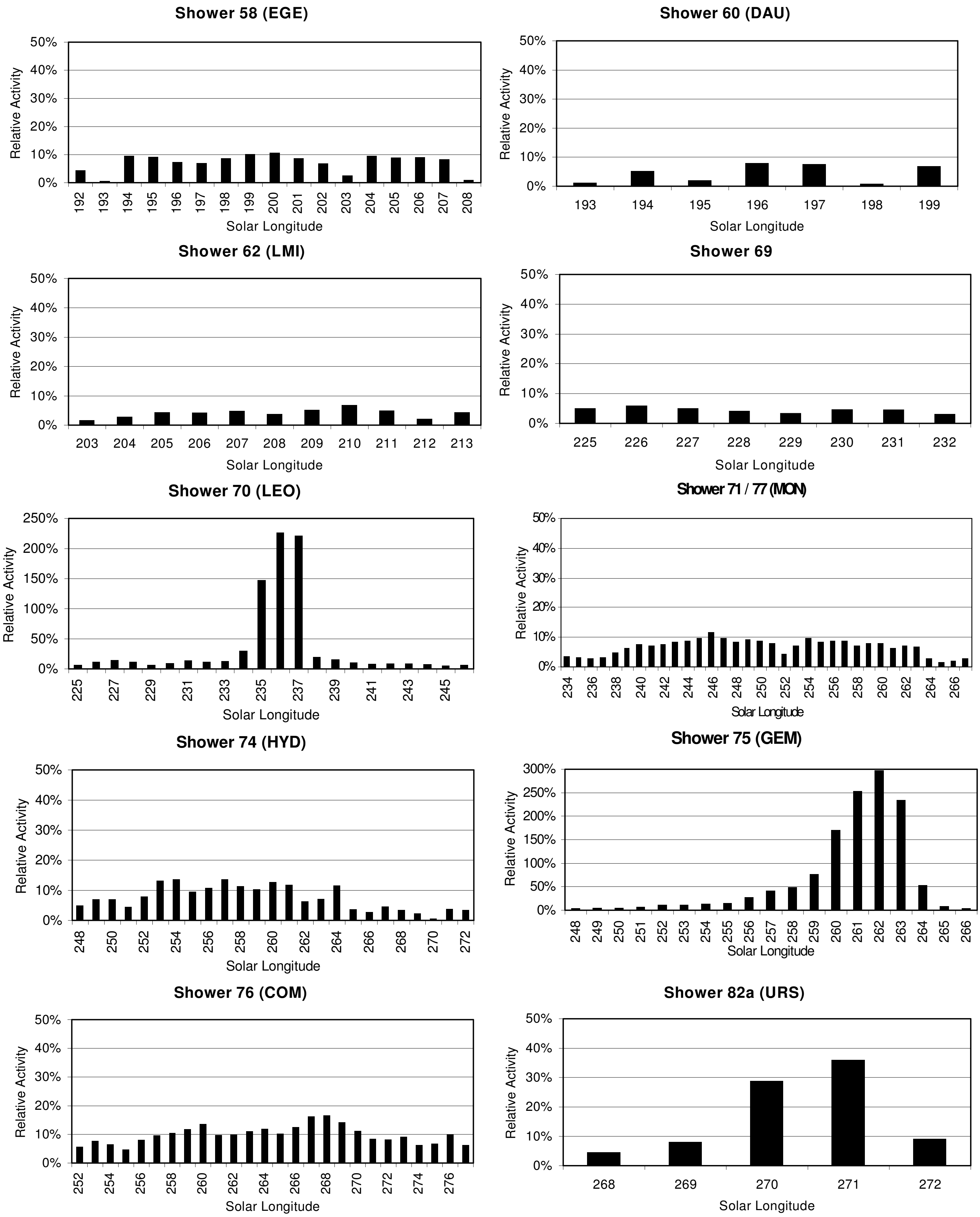

Figure 6: *Activity graphs for selected meteor*

Final remarks
Three meteor showers from the IMO Working List with declinations larger than –20° were not found, namely the delta Leonids, Draconids, and alpha Monocerotids. The latter two can be explained easily – they did not meet the minimum duration criterion in the meteor shower search. In fact, the June-Bootids, Aurigids, and Ursids did not meet this criterion either, but they clearly showed up when the number was reduced to five solar longitude intervals. For this reason, they were added to the shower list (Table 2).

With about 15,000 meteor records from two Australian observers, the data set for the southern hemisphere makes up for less than ten percent of the whole database. Still, it is remarkable that beside the Antihelion and Apex Source not even a single meteor shower with a declination below –20° was found.

Only one of the detected shower had a velocity greater than 65 km/s. Figure 7 shows the distribution of the computed vs. the expected velocity for known showers. The solid line depicts equal values. It is obvious, that the velocity is systematically underestimated for fast meteor showers. The reason for that deviation is not yet known.

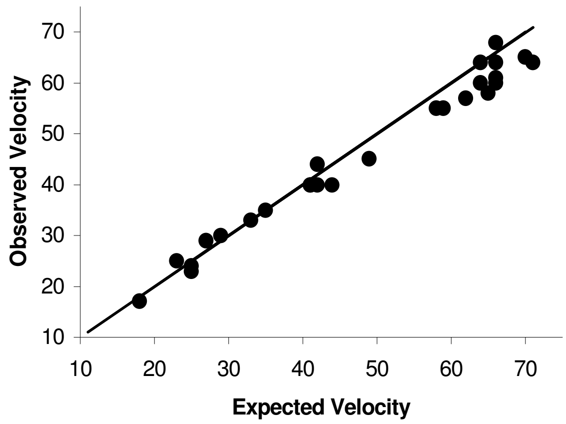

Figure 7: *Observed vs. expected velocity for known meteor showers.*

Conclusions
The new IMO Working List of Meteor Showers presented by Arlt and Rendtel (2006) is largely confirmed by this analysis. However, a number of significant discrepancies (e.g. KCG, AUR, COM and MON) need to be sorted out and corrections (especially with respect to the activity interval and radiant position of meteor showers) should take place. Many of the unknown showers presented in this analysis will be detectable by visual observers and should become the target of further investigation.

The analysis procedure presented here proved to be useful for detecting meteor showers that are active for at least a week. The software can be used to detect short-term meteor outburst, too, but that will require tighter filter criteria to discerne between real showers and statistical fluctuations.

Even though single-station video observations have certain limits compared to double and multi-station observations, they have proven to be useful for meteor shower analysis. Since they are easier to obtain, single station data outnumber the other by far, which makes them especially useful for the determination of activity profiles.

References

Arlt R. (1992). „The software Radiant“. *WGN*, **20**, 62-69.

Arlt R. (2003). “Radiant ephemeris for the Perseid meteor shower”, *WGN*, **31**, 19-28.

Arlt R. and Rendtel J. (2006). “A new Working List of meteor showers”, *WGN*, **34**, 77-84

Gural P. (1999). „A Rigorous Expression for the Angular Velocity of a Meteor“, *WGN*, **27**, 111-114.

Triglav-Cekada M. and Arlt R. (2005). „Radiant ephemeris of the Taurid meteor complex“. *WGN*, **33**, 41-58.

Rendtel J., Arlt R. and McBeath A. (Eds). Handbook for visual meteor observers. IMO Monograph No. 2, 1995.